Two-Dimensional Numerical Simulation of Shear-Layer Optics

Y. P. Tsai* and W. H. Christiansen†
University of Washington, Seattle, Washington 98195

Two-dimensional Euler equations are solved directly using the second-order, explicit, MacCormack predictor-corrector and Godunov methods alternately for the investigation of free-shear-layer optical properties. The optical effects of coherent structures in the mixing layer are identified. As expected, far-field optical quality of a laser beam is degraded the most when a laser beam passes through the edge of the large eddies. The far-field optical performance can be improved significantly by controlling the coherent structures in the mixing layer. The growth of shear layer is retarded by fundamental frequency forcing, and it is found the Strehl ratio is the highest in the nongrowth region.

I. Introduction

THE plane free shear layer generated by the mixing of two coflowing fluid streams is geometrically simple and is illustrated in Fig. 1. This simple flow configuration is important in mixing processes and is encountered in many other engineering applications. The extraction of power from high-power gas lasers, for example, often involves passing the beam through the interface between gases of different indices of refraction. Shear layers can produce random phase errors in the beam that can substantially reduce the maximum intensity to which the beam can be focused. The main purpose of this research is to understand the factors which influence optical degradation and to make useful predictions or correlations with respect to the flow parameters.

In order to understand the optical properties of the shear layers, it is necessary to understand their basic fluid mechanics. Many recent experiments have confirmed that large-scale coherent structures are intrinsic features of a plane mixing layer over a wide range of Reynolds numbers.[1,2] The plane mixing layer consists of an array of large eddies of concentrated spanwise vorticity. These quasi-two-dimensional large rollers are responsible for the transport of mass and momentum. In the past, the investigations of shear-layer optical properties were based on the assumptions that the natural shear layers were stationary and isotropic. There has been no study of the optical effect of large-scale structures which exist during the course of shear-layer development. One purpose of this work is to identify the optical effect of coherent structures. The features of the far-field intensity distribution pattern are caused by the large eddies as evidenced by experiments,[3] and this is further confirmed by this simulation. It is found experimentally that the shear-layer flow pattern can be altered easily by introducing external perturbations near the point of initial mixing.[4,5] Since the spreading rate and the density profile can be changed drastically by perturbing at a particular frequency with appropriate amplitude, then a concomitant question arises: could the optical effect of the shear layer be controlled, and how? Another purpose of this research is to seek out the method of improving optical performance in the far-field by controlling of the mixing layer.

Since the basic vortex dynamics in a shear layer are essentially inviscid, it is expected that significant results can be obtained by simulating the Euler equations. By alternating the MacCormack explicit, predictor-corrector and Godunov schemes,[6,7] the two-dimensional Euler equations can be solved directly and the density field obtained for optical studies. In Sec. II, we discuss the numerical method, initial conditions, and boundary conditions briefly. A detailed description of this numerical algorithm will be given in a separate paper. In Sec. III, the fluid dynamical statistics of the computations are given for both "natural" (to simulate a naturally developing, free shear layer, artificial perturbations are needed; see Sec. II) and forced shear layers. These results are compared with available experimental or numerical data for validation purposes. Optical statistics are presented in Sec. IV in parallel with a discussion of the physics upon which the optical effects of coherent structures are understood.

II. Governing Equations and Numerical Method

Based on the assumptions that there are no external heat addition and body forces, the compressible Euler equations in two-dimensional Cartesian coordinates can be written as

$$\frac{\partial \boldsymbol{U}}{\partial t}+\frac{\partial \boldsymbol{F}}{\partial x}+\frac{\partial \boldsymbol{G}}{\partial y}=0 \tag{1}$$

where $\boldsymbol{U}$, $\boldsymbol{F}$, and $\boldsymbol{G}$ are vectors given by

$$\boldsymbol{U}=\begin{bmatrix}\rho\\ \rho u\\ \rho v\\ e\end{bmatrix},\quad \boldsymbol{F}=\begin{bmatrix}\rho u\\ \rho u^2+p\\ \rho uv\\ (e+p)u\end{bmatrix},\quad \boldsymbol{G}=\begin{bmatrix}\rho v\\ \rho uv\\ \rho v^2+p\\ (e+p)v\end{bmatrix}$$

Here x is the streamwise coordinate, and y is the cross-stream coordinate (see Fig. 1). The equations written in conservation law form represent the conservation of mass, momentum, and total energy of inviscid fluid motions. The variables ρ, ρu, ρv, and e are mass, streamwise momentum, cross-stream momentum, and total energy, respectively, all per unit volume. The variable, p, is the pressure. For an ideal gas, the pressure is related to the equation of state

$$p=(\gamma-1)\rho\varepsilon \tag{2}$$

where ε is the specific internal energy and γ is the ratio of the specific heats, i.e., $\gamma=c_p/c_v$. Throughout this paper the value of γ is taken as 1.40.

The numerical code used in the current work is intended for the direct simulation of the two-dimensional compressible Euler equations [Eq. (1)] with no subgrid scale turbulence

Received Sept. 8, 1989; revision received Dec. 4, 1989.

*Graduate Student, Department of Aeronautics and Astronautics.
†Professor, Department of Aeronautics and Astronautics. Associate Fellow AIAA.

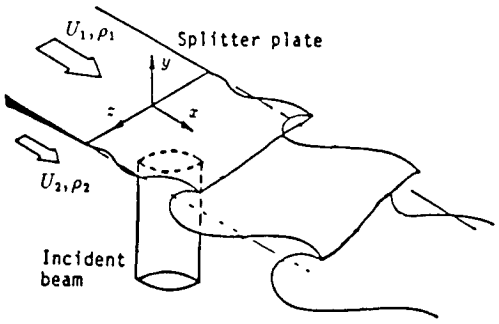

Fig. 1 Flow configuration and geometry.

model. The code uses finite volume techniques, which involve alternating in time the second-order, explicit MacCormack and Godunov methods. The state variables ρ, u, v, and e are calculated at the center of each computational cell, which is square mesh. A grid system at resolution of 200×50 is adopted. The computational domain is 16 cm long and 4 cm high. (Note that there exists a scaling relationship in this simulation, e.g., if all the length scales in the system are increased by a factor "M," the calculated results can be interpreted as having all frequency components reduced by the same factor "M" provided that all the other parameters are kept the same.)

Two air streams are modeled, each with different enthalpy, so that the density ratio is 1.1 at a velocity ratio of 0.5. The two freestream velocities are $U_1 = 7.04 \times 10^3$ cm/s ($M = 0.2$) and $U_2 = 3.52 \times 10^3$ cm/s; the densities are $\rho_1 = 1.2019 \times 10^{-3}$ g/cm^3 and $\rho_2 = 1.1\rho_1$. A hyperbolic-tangent velocity profile is adopted for the initial streamwise velocity distribution at the splitter plate such that the initial momentum thickness of the shear layer is 0.04 cm. However, in the initial density profile, there is a discontinuity at the contact surface. The pressure everywhere is 1 atm, and the y component of the velocity is zero.

Both mass flux and energy flux are kept constant as the inflow boundary conditions. Based on the hypothesis that the top and bottom boundaries are streamlines, the numerical boundary conditions used there are $v = 0$ and $\partial q/\partial y = 0$ where q is ρ, u, or e. For the outflow boundary condition, the pressure is assumed to be constant.

It has been shown that in order to resolve the large-scale structures in a mixing layer using an Euler code, unsteady boundary conditions must be applied.[8] In this case, at the inlet plane, a periodic forcing is introduced to simulate the "natural" mixing layer. The forcing frequencies consist of the fundamental frequency and the first three subharmonics of the shear layer. The fundamental frequency satisfies the Strouhal number criterion which is derived from Rayleigh's inviscid, linear stability theory.[9] In this case, the fundamental frequency is 4.227 kHz. Furthermore, the forcing is modified by incorporating random phases to the Rayleigh model to simulate random pairing of two neighboring vortices.[10]

III. Fluid Mechanical Results and Discussions

Figure 2 shows a sequence of instantaneous flow visualizations of the density field, and Fig. 3 is that of the vorticity distributions for the natural shear layer. The time interval Δt between the consecutive pictures is 0.168 ms. These figures clearly show the pairing phenomena between two vortices. Experimental evidence of the pairing process was observed and reported in many sources.[1,2] After the merging interactions among neighboring eddies, the newly formed large vortex convects downstream at nearly constant velocity, which is nearly the average of the two freestream velocities. This is verified by measuring the distance traveled by the center of large eddy during the time interval $\Delta t = 0.168$ ms in Figs. 2 and 3. The physical explanation is that the vortex sheet downstream of the trailing edge of the separation plate

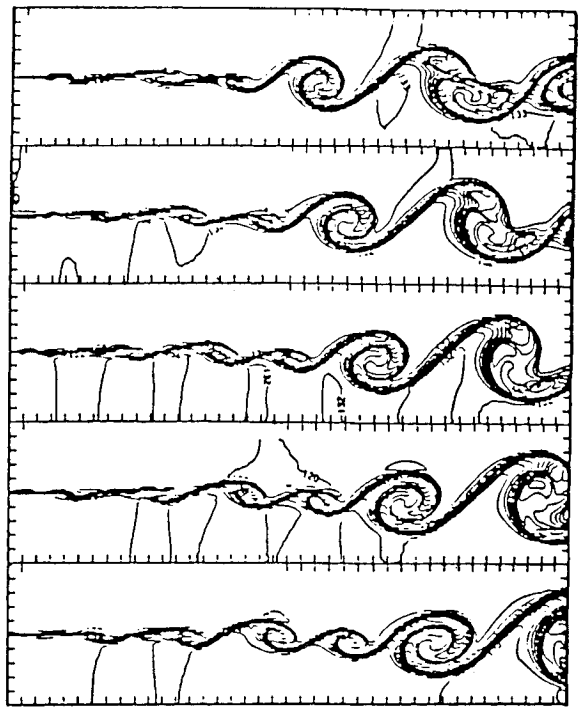

Fig. 2 Isodensity contour plots for the natural shear layer; $\Delta t = 0.168$ ms.

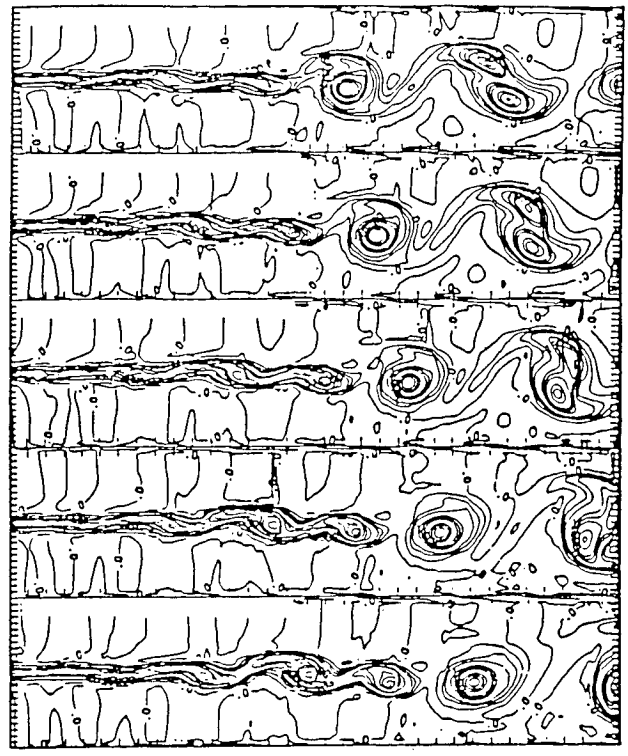

Fig. 3 Isovorticity contour plots for the natural shear layer; $\Delta t = 0.168$ ms.

rolled up into vortices via the Kelvin-Helmholtz instability mechanism. However, these spanwise vortex cores are unstable to subharmonic disturbances and then merge with each other to form a larger structure. This vortex amalgamation process occurs randomly in space and time, and it is responsible for the linear growth of the mixing layer. The growth rate calculated is 0.120 for the natural shear layer with velocity ratio 0.5 and density ratio 1.1; while that obtained using the incompressible formula derived by Papamoschou and Roshko[11] is 0.114.

In the plane free shear layer, the size of the coherent structures is comparable to the transverse length scale of the mixing layer. The time scale of vortex pairing is too short for significant viscous effects; therefore viscous effects are negligible, and the coherent structure dynamics are inviscid in nature. The adjacent structures are connected by braids which are regions of low vorticity and highly strained. Examining these figures carefully, it is found that the center of the shear layer moves toward the low-speed side. There are more irrotational fluid particles entrained from the high-speed side than that from the lower-speed side in the mixing region. Entrainment asymmetry is an important feature of the spatial shear layer, and this result is consistent with the experimental evidence[12] and other numerical simulations.[13]

In the fully developed region ($x > 8$ cm in this case), statistics of the fluid dynamical variables such as streamwise velocity, rms u fluctuations and rms v fluctuations show that the flow is self-similar. Furthermore the magnitude of these perturbations and the mean Reynolds stress are all of the correct magnitude and distribution.[5] An example of the mean Reynolds stress distribution is shown in Fig. 4a for the case of Fig. 2. An example power spectral distribution is also shown in Fig. 5.[14] Note that the distribution is fairly continuous. Subsequent calculations show that the spectrum moves toward lower frequencies with streamwise distance, and new frequencies are continually generated, fully suggestive of that for the mixing layer. On the average, the size of structures and their mean spacing increase with distance downstream of the initial point of mixing, which is required by the similarity properties of the mean flow. The mean spacing between the large eddies is approximately equal to $0.3x$, which is consistent with the experimental analysis of Brown and Roshko.[1] The similarity property is another important feature of the fully developed free shear layer and which is observed in many experiments.[1]

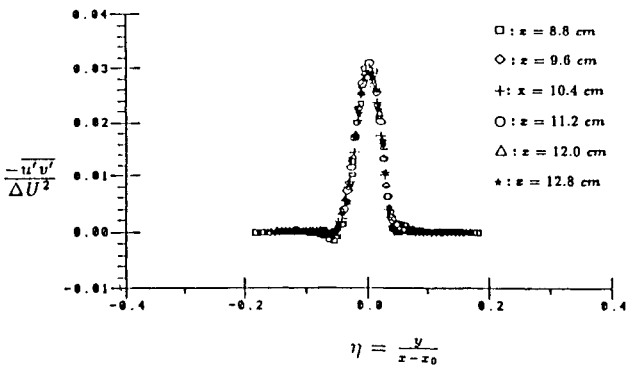

a) Reynolds stress for the natural shear layer

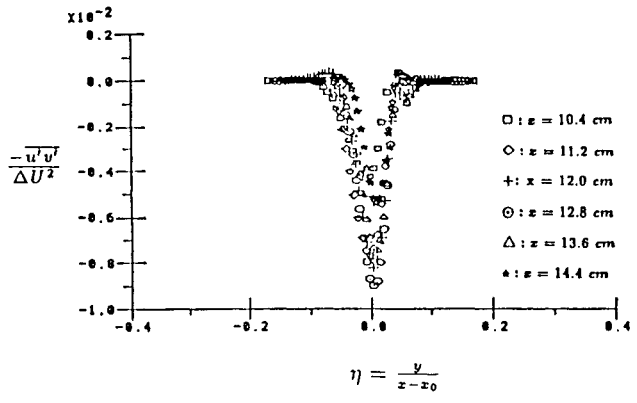

b) First subharmonic frequency forcing

Fig. 4 Lateral distribution of Reynolds stress for the shear layer; $\lambda_u = 0.5$, $\lambda_\rho = 1.1$.

For the forced cases, Fig. 6a shows an example of a snapshot picture of a density field under fundamental frequency forcing. Figure 6b is also the instantaneous isodensity plot, but the forcing frequency is at the subharmonic frequency. It is seen that in these forced cases, there is a region downstream of the splitter plate within which the shear layer stops growing. Vortex pairing is suppressed within this "non-growing" region, and calculations indicate that the growth rate of the time-averaged momentum thickness is zero in this region. For the case of fundamental frequency forcing, this behavior occurs earlier in space; while for the subharmonic surging, the mixing layer develops quickly due to merging of two vortices and then growth stops. In this region of zero growth rate, the calculated lateral distribution of the Reynolds stress is negative all across the layer as shown in Fig. 4b. This phenomenon was observed experimentally by Oster and Wygnanski[5] and also in the numerical simulation by Riley and Metcalfe.[15] The trends of the computed results to experiments and numerical results of others lend full confidence that the code has been validated satisfactorily.

IV. Shear-Layer Optical Statistics

Referring to Fig. 1, the diffraction coordinate system (x,z) is the finite aperture plane, and (x_0,z_0) is the system of observation plane in the far field (not shown). The two planes are parallel to each other, and L is the distance between them. Applying the Huygens-Fresnel principle and assuming that the Fraunhofer diffraction condition

$$L \gg \frac{\pi}{\lambda}(x^2 + z^2)$$

is satisfied, where λ is the wavelength of the beam, then the

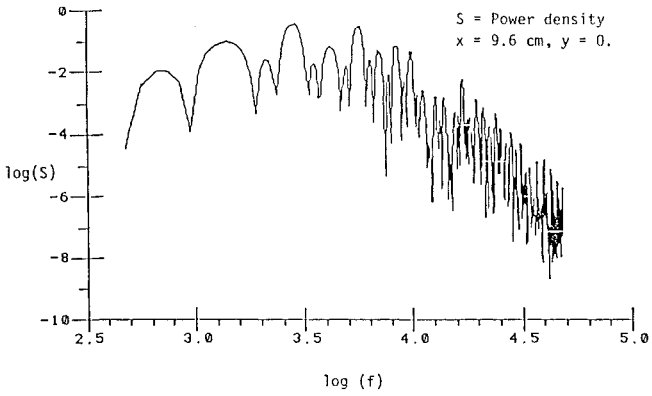

Fig. 5 Power density spectrum for the natural shear layer; $\lambda_u = 0.5$, $\lambda_\rho = 1.1$ and $x = 9.6$ cm, $y = 0$.

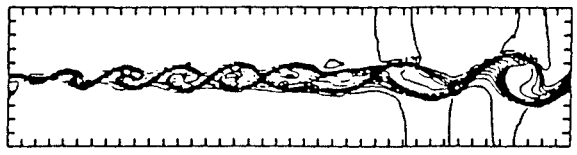

a) Forced by fundamental frequency

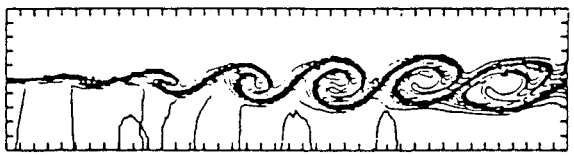

b) Forced by first subharmonic

Fig. 6 Instantaneous density plot for the forced shear layer.

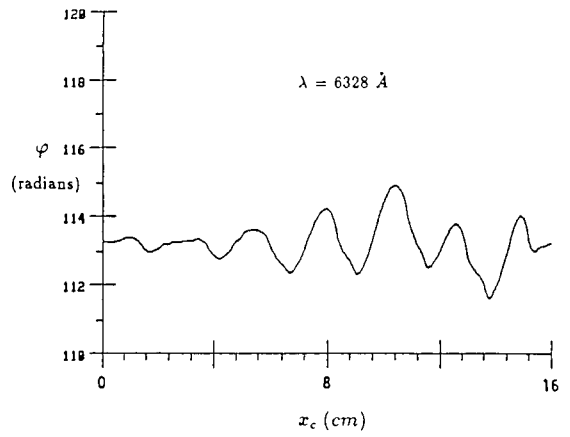

Fig. 7 Instantaneous optical phase variation for the natural shear layer.

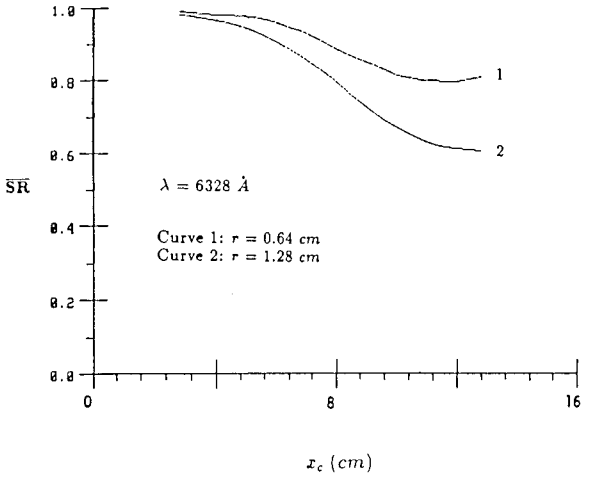

Fig. 8 Time-averaged Strehl ratio at different beam sizes for the natural shear layer; $\lambda_u = 0.5$, $\lambda_\rho = 1.1$.

electric field amplitude A at point (x_0,z_0) can be written as[16,17]

$$A(x_0,z_0) = \frac{1}{j\lambda L}\exp(jkL)\exp\left[j\frac{k}{2L}(x_0^2+z_0^2)\right] \times \int\int_{-\infty}^{+\infty} A(x,z)\exp\left[-j\frac{2\pi}{\lambda L}(x_0x+z_0z)\right]dx\,dz \qquad (3)$$

where $j=\sqrt{-1}$, and $k=2\pi/\lambda$ is the wave number. The integral in the preceding equation is simply the two-dimensional Fourier transform of the aperture function $A(x,z)$, assessed at spatial frequencies $f_{x_0}=x_0/\lambda L$ and $f_{z_0}=z_0/\lambda L$. The far-field intensity profile is the modulus square of the Fourier transform of the near-field incident wave distributions. For a uniform, monochromatic, and coherent circular beam with no aberrations, the far-field intensity distribution pattern is circular, which is called the Airy pattern. A phase shift of π between the left half and right half of the circular beam will produce two symmetric bright spots and zero intensity on the axis in the far field, but the peak intensity is only 47% that of the diffraction limited case. A phase error magnitude in the beam of this order can be quite common during the interaction between laser and shear layer. So it is clear that phase distortion of a coherent light beam plays a very important role in determining the far-field properties of the beam.

The optical effects of the shear layer are calculated by passing a laser beam through it with circular aperture and uniform phase. The far-field focal plane intensity distributions measure the optical quality of the shear layer. The Strehl ratio, SR, which is defined as the ratio of the maximum light intensity of the diffraction pattern to that of the same optical system without aberrations, will be used to evaluate the optical quality quantitatively.

Considering a thin lens approximation and assuming no absorption of light within the shear layer, the only effect of the layer is to change the phase of the incident coherent wave. The index of refraction for a gas is given by

$$n = 1+\beta\frac{\rho}{\rho_s} \qquad (4)$$

where β is the Gladstone-Dale constant, ρ is the gas density, and ρ_s is the density at standard conditions. The phase change of the laser beam traversing the mixing layer is then given by

$$\varphi(x,t) = \frac{2\pi}{\lambda}\int_0^w \beta\frac{\rho(x,y,t)}{\rho_s}\,dy \qquad (5)$$

where w is the thickness of layer. For air at standard conditions $\beta/\rho_s = 0.244\ \text{cm}^3/\text{g}$. In this simulation, λ is chosen equal to 6328 Å. A typical example which shows the variation of phase error φ as a function of the streamwise coordinate x for an instantaneous natural mixing layer is illustrated in Fig. 7. The variation of φ grows larger downstream, and the turbulent scale also increases with x. This is correlated with the linear growth of the layer. Since the shear layer is two-dimensional, φ is independent of z. Suppose now the shear layer is uniformly illuminated by a circular, normally incident, monochromatic plane wave of unit amplitude. Then we have

$$A(x,z,t) = T(x,z)e^{j\varphi(x,t)} \qquad (6)$$

where $T(x,z)$ is the amplitude transmittance function defined by

$$T(x,z) = \begin{cases} 1 & \text{if } x^2+z^2 \le r^2 \\ 0 & \text{otherwise} \end{cases}$$

and r is the radius of the aperture (or radius of the beam). Carrying out the two-dimensional Fourier transform integration, first the field amplitude $A(x_0,z_0)$ at a particular point (x_0,z_0) in the far field and then the far-field intensity at (x_0,z_0) are obtained. As the time scale of fluid motion is much longer than the time for light to traverse the layer, one can calculate the far-field intensity distribution due to the flow at a fixed instant and recalculate it at the next instant and so on. Repeating this many times, the resulting ensemble averaged far-field intensity distribution would represent the time-averaged distribution. The time-averaged Strehl ratio SR is plotted in Fig. 8 as a function of x_c at two different beam sizes, where x_c is the streamwise location of the beam center. Beam degradation is more severe for the larger size beam, and both appear to approach an asymptotic value. For the smaller beam, this trend starts earlier. The principal mechanism of beam degradation is explained as follows. The mixing layer produces random phase fluctuations in the incident beam and results in wavefront aberrations in the near field. The beam coherency is reduced, and then the peak intensity is lowered in the far field. For large beams, the scale of the fluid fluctuations (turbulent scale) is smaller than the beam diameter. Wide angle scattering due to these structures removes optical energy from the beam and spreads the intensity profile in the far field. However, for small beams in relation to the fluid scale, most of the degradation is due to wavefront tilt.

The far-field intensity contour plots are shown in Figs. 9 and 10 for the same beam sizes ($r = 2.56$ cm) but at different locations in a natural shear layer ($x_c = 7.96$ cm in Fig. 9 and $x_c = 10.76$ cm in Fig. 10). Note that the far-field coordinates with respect to the center of the incident beam (x_0,z_0) are expressed in terms of $\lambda L/D$, where D is the diameter of the

beam. In Fig. 9, the scale of the fluid fluctuations is smaller than the beam size, and there are two lobes of almost equal peak value in the scattered far-field intensity pattern. In Fig. 10, the center of the beam moves farther downstream where the size of the flow disturbance is a fraction of the size of the beam, and then the shape of the intensity distribution is only distorted.

Figure 11 gives a typical example plot of the instantaneous Strehl ratio for the natural shear layer. The corresponding density field is put at the top of the figure for reference. It indicates that, at the edge of coherent structures, optical degradation increases to a local maximum while within the braid, beam degradation is significantly reduced. The reason is that in the vicinity of the edge of a large eddy, the phase variation is large. The bigger the vortex, the larger is the magnitude of the variation. In the region of a braid or vortex core, the density distribution is relatively uniform, and these regions generate less optical degradation. Using the electronic imaging system which consists of a charge coupled device (CCD) camera array of 256×256 photodiodes, an image processor, and a microcomputer, experimental measurements of the Strehl ratio can be carried out.[3] Although the experimental results include the effects due to molecular diffusion and streamwise vortices, which appear beyond the so-called "transition region,"[19] the general trends of the numerical simulation and experiment are similar.

The simplest and most natural way of modifying the mixing layer is to perturb the layer by external, periodic disturbances. Forcing with fundamental or subharmonic frequency produces controlled coherent structures. In the nongrowing region of the shear layer, amalgamation of neighboring vortices are inhibited, and the mixing layer consists of an array of large eddies in the lateral direction with no interactions. These large eddies, which are equal in size, result in the amplitude of the phase variation being small [see Eq. (5)], which in turn improves the optical performance in the far field. Figure 12 presents this important result. Comparing Figs. 8 and 12, we find that beam degradation is indeed reduced significantly within the nongrowing region. Referring to Fig. 8, for the natural shear flow at $x_c = 12$ cm and beam size $r = 1.28$ cm, the Strehl ratio is 0.6 approximately, whereas in the case of corresponding subharmonic forcing, the Strehl ratio is above 0.9, which is a significant improvement.

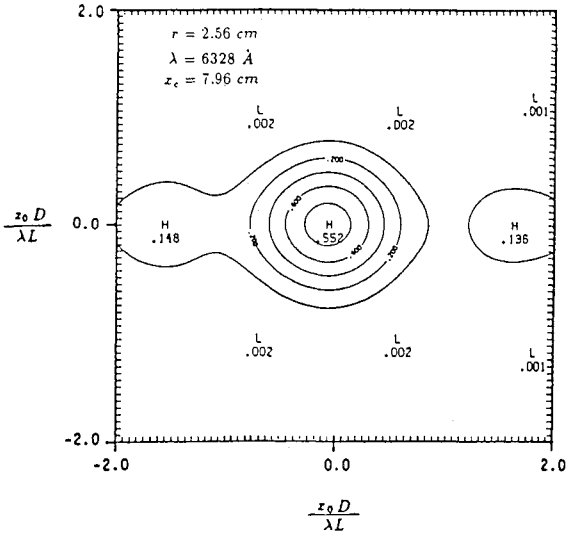

Fig. 9 Instantaneous far-field intensity distribution; $x_c = 7.96$ cm, $r = 2.56$ cm.

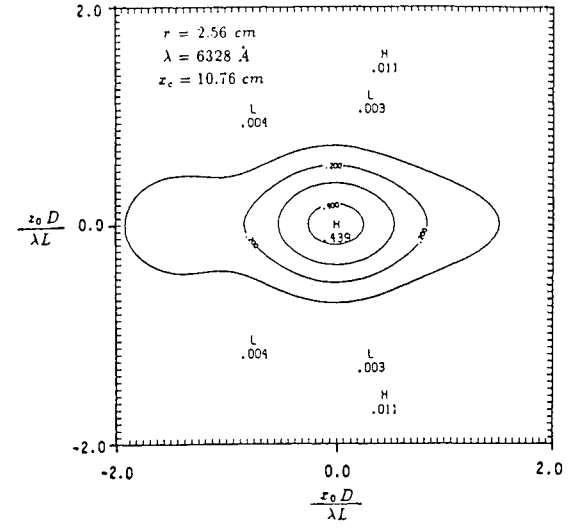

Fig. 10 Instantaneous far-field intensity distribution; $x_c = 10.76$ cm, $r = 2.56$ cm.

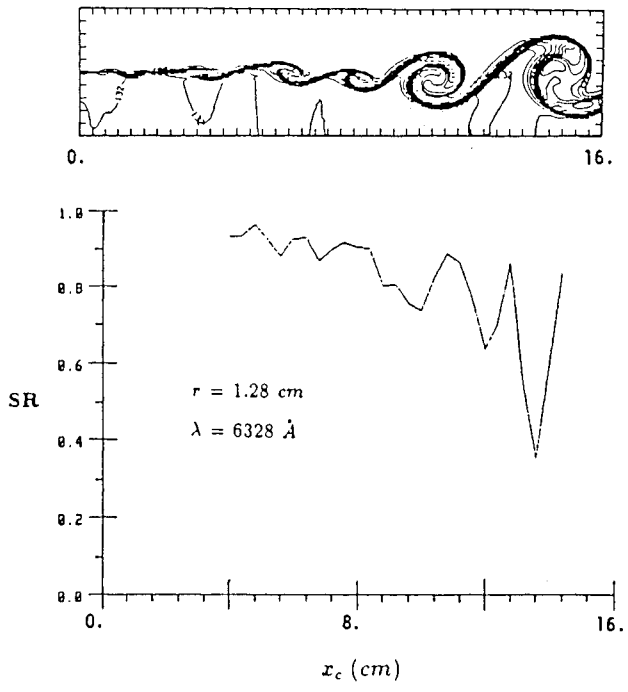

Fig. 11 Instantaneous Strehl ratio for the natural shear layer.

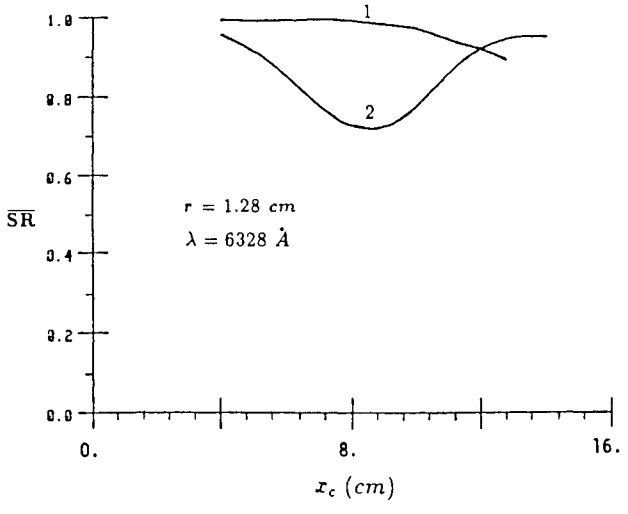

Curve 1: forced by fundamental freq.
Curve 2: forced by first subharmonic

Fig. 12 Time-averaged Strehl ratio at different forcing frequencies.

The thickness of the mixing layer in the region of no growth is controlled by the forcing frequency and increases with decreasing forcing frequency. This explains why forcing at the fundamental frequency yields a higher value in Strehl ratio than at subharmonic forcing, provided that the beam sizes are the same. The shear layer excited by the fundamental frequency has a region of zero growth rate near the initial point of mixing, but the region for the first subharmonic forced case is farther downstream from the initial point of mixing (see Figs. 6a and 6b). If beam performance improvement is needed in the region near the point of mixing, the method of fundamental frequency forcing should be applied; otherwise the methods of subharmonic forcing may be used (see Fig. 12).

V. Conclusions

A numerical simulation of the spatially developing plane shear layer and its optical properties have been performed for the free shear with velocity ratio 0.5 and density ratio 1.1. Introducing random phases to the forcing modes makes the simulation of a natural mixing more realistic. In the forced mixing layer, a region of nongrowth was identified, which is crucial to optical quality improvement in the far field. It is found that, at the edge of coherent structures, the optical quality is the worst. For a relatively large size beam, degradation is correlated to the turbulence structures of the mixing layer. For a small size beam, however, the main degradation mechanism is wavefront tilt. Beam degradation is found to increase with increasing beam diameter and increasing turbulence integral scale. The Strehl ratio can be significantly enhanced by retarding the growth of the mixing layer via fundamental frequency forcing. Numerical simulation provides a method of which it is easy to change the flow and optical parameters for a systematic investigation of the interaction between shear layer and lasers. Additional work in this area is forthcoming.

Acknowledgments

The authors would like to thank J. J. Riley and S. D. Eberhardt and especially D. W. Bogdanoff for their suggestions in simulating the flowfield. Part of the work is completed using SDSC CRAY X-MP, which is gratefully acknowledged.

References

[1]Brown, G. L., and Roshko A., "On Density Effects and Large Structures in Turbulent Mixing Layers," *Journal of Fluid Mechanics*, Vol. 64, June 1974, pp. 775–816.

[2]Winant, C. D., and Browand, F. K., "Vortex Pairing, Mechanism of Turbulent Mixing Layer Growth at Moderate Reynolds Number," *Journal of Fluid Mechanics*, Vol. 63, April 1974, pp. 237–255.

[3]Chew, L., private communication, Dept. of Aeronautics of Astronautics, Univ. of Washington, Seattle, WA, 1989.

[4]Ho, C. M., and Huang, L. S., "Subharmonics and Vortex Merging in Mixing Layers," *Journal of Fluid Mechanics*, Vol. 119, June 1982, pp. 443–473.

[5]Oster, D., and Wygnanski, I., "The Forced Mixing Layer between Parallel Streams," *Journal of Fluid Mechanics*, Vol. 123, Oct. 1982, pp. 91–130.

[6]MacCormack, R. W., "The Effect of Viscosity in Hypervelocity Impact Cratering," AIAA Paper 69-354, 1969.

[7]Holt, M., *Numerical Methods in Fluid Dynamics*, Springer-Verlag, Berlin, 1977, pp. 29–37.

[8]Chien, K. Y., Ferguson, R. E., Collins, J. P., Glaz, H. M., and Kuhl, A. L., "A Study of Mixing in Forced Shear Layers with an Euler Code," AIAA Paper 87-1318, 1987.

[9]Ho, C. M., and Huerre, P., "Perturbed Free Shear Layers," *Annual Review of Mechanics*, Vol. 16, 1984, pp. 365–424.

[10]Sandham, N. D., and Reynolds, W. C., "Some Inlet Plane Effects on the Numerically Simulated Spatially Developing Two Dimensional Mixing Layer," Sixth Symposium on Turbulent Shear Flows, Sept. 1987, Toulouse, France, pp. 22-4-1–22-4-6.

[11]Papamoschou, D., and Roshko, A., "Observations of Supersonic Free Shear Layers," AIAA Paper 86-0162, Jan. 1986.

[12]Koochesfahani, M. M., Dimotakis, P. E., and Broadwell, J. E., "Chemically Reacting Shear Layer," AIAA Paper 83-0475, 1983.

[13]Grinstein, F. F., Oran, E. S., and Boris, J. P., "Numerical Simulations of Asymmetric Mixing Layer in Planar Shear Flows," *Journal of Fluid Mechanics*, Vol. 165, April 1986, pp. 201–220.

[14]Tennekes, H., and Lumley, J. L., *A First Course in Turbulence*, The MIT Press, Cambridge, MA, 1972, pp. 214–215.

[15]Riley, J. J., and Metcalfe, R. W., "Direct Numerical Simulation of a Perturbed, Turbulent Mixing Layer," AIAA Paper 80-0274, 1980.

[16]Goodman, J. W., *Introduction to Fourier Optics*, 1st ed., McGraw-Hill, New York, 1968, p. 61.

[17]Born, M., and Wolf, E., *Principles of Optics*, 6th ed., Pergamon Press, New York, 1980, p. 395.

[18]Liepmann, H. W., and Roshko, A., *Elements of Gasdynamics*, 1st ed., Wiley, New York, 1957, p. 154.

[19]Breidenthal, R., "Structure in Turbulent Mixing Layers and Wakes Using a Chemical Reaction," *Journal of Fluid Mechanics*, Vol. 109, Aug. 1981, pp. 1–24.